Journal of Applied Physics

Electron density measurement of inductively coupled plasmas by terahertz time-domain spectroscopy (THz-TDS)

Cite as: J. Appl. Phys. **110**, 073303 (2011); https://doi.org/10.1063/1.3633488
Submitted: 23 June 2011 . Accepted: 22 July 2011 . Published Online: 05 October 2011

Ayumi Ando, Tomoko Kurose, Vivien Reymond, Katsuhisa Kitano, Hideaki Kitahara, Keisuke Takano, Masahiko Tani, Masanori Hangyo, and Satoshi Hamaguchi

Electron density measurement of inductively coupled plasmas by terahertz time-domain spectroscopy (THz-TDS)

Ayumi Ando,[1] Tomoko Kurose,[1] Vivien Reymond,[1,2] Katsuhisa Kitano,[1] Hideaki Kitahara,[3] Keisuke Takano,[3] Masahiko Tani,[4] Masanori Hangyo,[3] and Satoshi Hamaguchi[1,a)]

[1]*Center for Atomic and Molecular Technologies, Osaka University 2-1 Yamadaoka, Suita, Osaka 565-0871, Japan*
[2]*ENSPS, Université de Strasboug, Boulevard Sébastien Brant BP10413 67412 Illkirch Cedex, France*
[3]*Institute of Laser Engineering, Osaka University 2-6 Yamadaoka, Suita, Osaka 565-0871, Japan*
[4]*Research Center for Development of Far-Infrared Region, University of Fukui 3-9-1 Bunkyo, Fukui City, Fukui Prefecture 910-8507, Japan*

(Received 23 June 2011; accepted 22 July 2011; published online 5 October 2011)

The electron densities of argon inductively coupled plasmas were measured by terahertz time-domain spectroscopy (THz-TDS). At a low pressure, the electron densities were also measured with a Langmuir-type double probe and the validity of THz-TDS electron-density measurement in a plasma has been corroborated. As the input radio-frequency (RF) power increases, the plasma density and gas temperature increase, which makes the probe measurement less reliable or even impossible, due to the large heat load to the probe surface. On the contrary, the THz-TDS measurement is unaffected by the gas temperature and becomes more reliable due to the higher electron density at higher input power for plasma generation. © *2011 American Institute of Physics*. [doi:10.1063/1.3633488]

I. INTRODUCTION

Electromagnetic (EM) waves whose frequency is approximately in the range of 0.1–10 THz are called terahertz (THz) waves. Since Auston *et al.*[1] invented a technique to emit and detect EM waves in the THz frequency domain with the use of photoconductive antennas and a femtosecond laser, terahertz time-domain spectroscopy (THz–TDS) has been rapidly developed as spectroscopy in the frequency range between microwave and infrared that had not previously been well explored.

In the THz-TDS technique, which will be explained in more detail in Sec. II for an experimental setup specific to our interest, the amplitude of EM waves are obtained as a function of time with sub-picosecond time-resolution, which then can be transformed to the frequency spectra. If a THz wave passes through a medium that interacts with it, its absorption or delay in the phase may appear in the frequency spectra. Since vibrational frequencies of large molecules and electron plasma frequencies of high-density plasmas can fall into the THz range, THz–TDS is expected to serve as a diagnostic tool for high-density plasmas and some molecular gases. Furthermore, due to its high time resolution, THz–TDS can provide time-resolved information for fast transient phenomena.

Jamison *et al.*,[2] Kolner *et al.*,[3,4] and Mics *et al.*[5] used THz–TDS to measure time evolution of the electron density for pulsed discharges at high pressures (10–760 Torr). Since a plasma typically has a frequency-dependent refractive index smaller than unity, an EM-wave that can be transmitted through a plasma exhibits a phase shift. As we shall see in Sec. II, deviation of the refractive index from unity is largest for the wave frequency just above the plasma frequency and therefore EM waves in the THz range are expected to be highly effective for the phase shift measurements of high density plasmas.

In Refs. 2–5 however, no discussion is provided on the corroboration of the validity of their electron density measurement based on THz–TDS using a different method for electron density measurements. Since no other practical method exists to measure the electron densities of transient high pressure plasmas, corroboration of the density measurement by THz–TDS remains difficult for such plasmas.

In our study, we applied THz–TDS to measure electron densities of standard inductively coupled plasmas (ICPs) for Ar at relatively low pressures with an RF frequency of 13.56 MHz and compared the results with the electron densities obtained from probe measurements of the same plasmas. Depending on the gas pressure and input RF power, the plasma density of an ICP can be high and reach the range of 10^{13} cm^{-3}, so we mostly examined discharge conditions for relatively high electron densities in this study to take advantage of THz–TDS spectroscopy. Since the bulk electron density of an ICP driven by an RF frequency is considered to be invariant in time, we measured the time-averaged electron density over many RF cycles by THz–TDS for each set of discharge parameters.

For collision frequencies, however, the pressure range we examined is much lower than that of the work by Jamison *et al.*[2] and the electron-neutral collision frequencies of our ICP Ar plasmas is on the lowest side of the GHz range. Therefore, the collisional absorption of the THz waves is expected to be undetectable in our experiments.

a)Author to whom correspondence should be addressed. Electronic mail: hamaguch@ppl.eng.osaka-u.ac.jp.

II. THz–TDS AS PLASMA DIAGNOSTICS

When an EM wave in the THz range passes through an unmagnetized plasma, the motion of electrons may be affected by the electric field, **E**, of the wave and is governed by the equation,

$$m\frac{d\mathbf{v}}{dt} = -e\mathbf{E} - \nu m\mathbf{v}, \tag{1}$$

where m, $\mathbf{v}$, e, and ν are the mass and velocity of electrons, elementary charge, and electron-neutral collision frequency, respectively. Assuming that ion motion can be ignored, the electrical conductivity of the plasma is derived from Eq. (1) as,

$$\sigma(\omega) = \frac{\varepsilon_0\omega_p^2}{i\omega + \nu},$$

and its dielectric constant is given by

$$\varepsilon(\omega) = \varepsilon_0\left(1 + \frac{\sigma(\omega)}{i\omega\varepsilon_0}\right),$$

where the frequency of the EM wave is given by ω, $\omega_p = \left(n_e e^2/\varepsilon_0 m\right)^{1/2}$ is the electron plasma frequency, n_e is the electron density, and ε_0 denotes the vacuum permittivity. The (complex) refractive index and wave number are then given, by definition, as $N_p = \sqrt{\varepsilon(\omega)/\varepsilon_0}$ and $k_p = \omega\sqrt{\varepsilon(\omega)\mu_0}$ with μ_0 being the vacuum permeability, i.e.,

$$k_p = k_0\left[\left(1 - \frac{\omega_p^2}{\omega^2+\nu^2}\right) - i\left(\frac{\omega_p^2}{\omega^2+\nu^2}\right)\frac{\nu}{\omega}\right]^{1/2},$$

where $k_0 = \omega/c$ is the wavenumber in vacuum with c being the speed of light in vacuum. The real ($\Re k_p$) and imaginary ($\Im k_p$) parts of k_p then satisfy,

$$\left(\Re k_p\right)^2 = \frac{k_0^2}{2}\left(1 - \frac{\omega_p^2}{\omega^2+\omega_p^2}\right)\left(\sqrt{1 + \frac{\omega_p^4}{\left(\omega^2+\nu^2-\omega_p^2\right)^2}\left(\frac{\nu}{\omega}\right)^2} + 1\right),$$

and

$$\left(\Im k_p\right)^2 = \frac{k_0^2}{2}\left(1 - \frac{\omega_p^2}{\omega^2+\omega_p^2}\right)\left(\sqrt{1 + \frac{\omega_p^4}{\left(\omega^2+\nu^2-\omega_p^2\right)^2}\left(\frac{\nu}{\omega}\right)^2} - 1\right).$$

The wave number changes from k_0 to k_p in the presence of the plasma and we denote the difference by $\Delta k = k_0 - k_p$.

If the frequency, ω, is sufficiently higher than the plasma frequency and collision frequency, i.e.,

$$\omega^2 \gg \omega_p^2,\ \nu^2, \tag{2}$$

then we have to the lowest order,

$$N_p = \sqrt{1 - \frac{\omega_p^2}{\omega^2}},$$

and

$$\Delta k = \frac{\omega}{2c}\left(\frac{\omega_p}{\omega}\right)^2. \tag{3}$$

Since the phase shift of the EM wave over an infinitesimal length, dx, is given by $\Delta k\,dx$, the phase shift over the entire plasma is given, in general,[2] by

$$\Delta\Phi = \int \Delta k\,dx,$$

where the integral is taken over the path of the EM wave in the plasma. If the conditions of Eq. (2) hold and the wave-number shift is given by Eq. (3), the phase shift is given by,

$$\Delta\Phi = \frac{L}{2c\omega}\frac{e^2\bar{n}_e}{\varepsilon_0 m}, \tag{4}$$

where L denotes the length of the EM wave path in the plasma and $\bar{n}_e$ is the line average of the electron density over the path, i.e.,

$$\bar{n}_e = \frac{1}{L}\int_0^L n_e(x)\,dx.$$

Equation (4) shows that the line-averaged electron density of the plasmas can be obtained from the measurement of the phase shift, $\Delta\Phi$, by THz–TDS. A highly ionized plasma whose density is in the range of 10^{12} cm^{-3} or lower satisfies the conditions (2) for THz waves and therefore, the phase shift obtained from THz-TDS for such a plasma is expected to be given by Eq. (4), i.e., inversely proportional to the wave frequency, ω.

III. EXPERIMENTAL SETUP

A. THz time-domain spectroscopy system

A schematic diagram of the THz-TDS system[6] used in this work is given in Fig. 1. A pump-probe method is employed for the measurement of the wave forms of THz

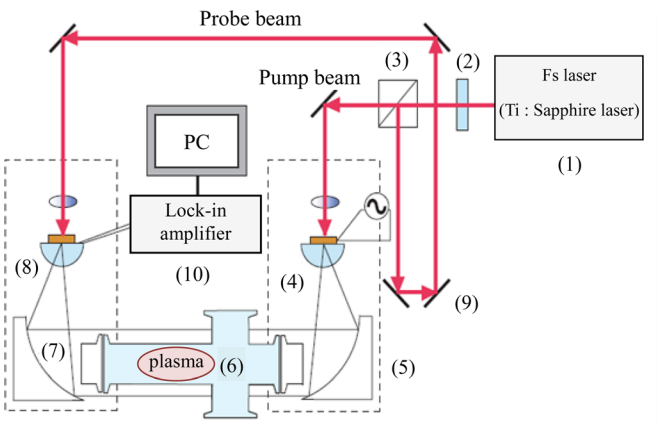

FIG. 1. (Color online) Setup of THz time domain spectroscopy and plasma chamber. Femtsecond laser (1), half-wave plate (2), beam splitter (3), THz emitter (4), off-axis parabolic mirror (5), plasma chamber (6), off-axis parabolic mirror (7), THz detector (8), optical time delay mirror (9), and lock-in amplifier (10).

pulses. The system consists of a femtosecond laser (1) (Tsunami mode locked titanium sapphire laser from Spectra Physics, Inc.) as the pulse source, an optical system that guides laser beams, the photoconductive antennas that emit or detect THz pulses, and another optical system that guides THz pulses between the photoconductive antennas. The laser beam is 800 nm in wavelength, 100 fs in pulse width, and 80 MHz in repetition frequency. The polarization direction of the laser is controlled by the half-wave plate (2) so that the pump and probe beam power is separated into a desired ratio by the polarizing beam splitter (3). The pump beam is directed to the emitter (4) for THz electromagnetic (EM) wave emission whereas the probe beam is directed to the detector (8) that detects incoming THz EM waves only when it is irradiated by a probe beam. The emitter is a dipole-type photoconductive antenna whose bandwidth is in the range from 0 to 3 THz. The detector is a bow-tie photoconductive antenna which is suitable for detecting a phase shift of 0.1 –0.5 THz for THz EM waves.[7] Both the emitter and detector are based on the design of Au/Ni/Ge electrodes formed on a photoconductive substrate with a low-temperature grown GaAs (LT-GaAs) layer (2–μm thick) on semi-insulating GaAs (SI-GaAs) (~0.4–mm thick). The electrode gap of the emitter antenna is 5 μm and biased by a peak-to-peak voltage of 60 V at 10 kHz. When the gap of the antenna electrodes on the emitter is irradiated by a laser light (i.e., pump beam) with photon energy higher than the band-gap energy of the semiconductor, photoexcited carriers (i.e., electrons and holes) are generated and accelerated by the bias voltage so that a small electric current flows in the semiconductor under the electrode gap. The EM waves generated by the time varying current are emitted as THz waves through a hyper-hemispherical high resistivity silicon lens attached to the emitter. The magnitude of the electric field of the emitted wave is proportional to the time derivative of the current density.

As shown in Fig. 1, the off-axis parabolic mirror (5) with a diameter of 1 in. and a focal length of 2 in. is used to collimate THz EM waves into a beam 1 in. in diameter, which is then directed to the plasma chamber (6). The THz EM waves that pass through the plasma chamber were then directed to the detector (8) by another off-axis parabolic mirror (7) with a diameter of 2 in. and a focal length of 2 in. The collected THz EM waves are then focused on the 5 μm electrode gap of the detector by a hyper-hemispherical high resistivity silicon lens attached to the detector.

The probe beam was delayed by the optical time delay mirror (9) before reaching the detector (8), shown in Fig. 1. When a probe beam and THz waves reach the detector simultaneously, photoexcited carriers are generated in the semiconductor of the detector and a current proportional to the oscillating electric field of the THz wave flows across the electrode gap. The measurement of this current provides information on the electric field of the incoming THz EM waves. The time dependence of the pulsed electric field is obtained from the measurement of the instantaneous fields of many pulses with scanning of the delay time, under the assumption that each pulse has nearly the same time-dependent wave form.

A lock-in amplifier (10) is required for the measurement of a current in the detector semiconductor on the order of nano amperes (nA) as a high signal-to-noise ratio. The THz pulses are modulated by a sinusoidal bias voltage on the emitter and synchronously demodulated at the detector.

B. Plasma chamber

A plasma discharge chamber is placed between the THz wave emitter and the detector, as indicated in Fig. 1. Figure 2 is a schematic diagram of the plasma chamber used in this study. It consists of a quartz tube cross (with both vertical and horizontal tubes being 140 mm long, 57 mm in outer diameter, and 52 mm in inner diameter) and an additional horizontal quartz tube (110 mm long, 57 mm in outer diameter, and 52 mm in inner diameter). Both quartz parts are connected with flanges and therefore the total length of the horizontal section is about 250 mm. A copper 3-turn antenna is wound around the horizontal tube of the cross and excited by a 13.56 MHz power supply with an appropriate impedance matching network to generate the ICPs in the chamber. The plasma chamber and antenna are enclosed in an aluminum box to prevent the RF signals from affecting other electronic instruments.

Pulsed THz EM waves are transmitted through the plasma via polyethylene windows that are attached to both ends of the horizontal section of the chamber. Polyethylene windows, rather than quartz or borosilicate glass windows, are selected because of the low refraction coefficient of polyethylene. The thickness of the polyethylene window is selected to be 30 mm in order to prevent THz EM waves reflected by the polyethylene window surface from affecting the pulse signal measurement. In this system, a reflection signal by the hyper-hemispherical silicon lens appears at around 300 ps after the detection of the THz pulse peak signal. With 30 mm polyethylene windows, reflection signals by the windows appear even after the reflection signals by the hyper-hemispherical silicon lens. This insures the time-dependent electric field measurement of THz waves for a duration of up to 300 ps, which provides sufficient low-frequency

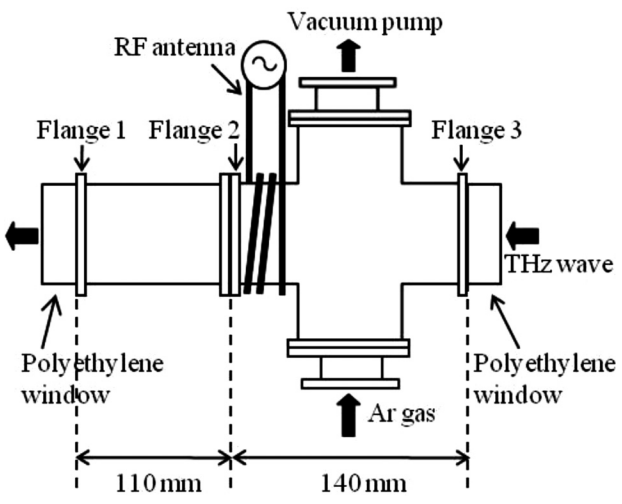

FIG. 2. Schematic diagram of the ICP discharge chamber used for THz–TDS.

components for the purpose of our THz-TDS. Note that polyethylene windows need to be placed away from the plasma in order to avoid damages caused by plasma sputtering.

In the experiments discussed in this paper, the plasma chamber was evacuated to 3 Pa by an oil-sealed rotary pump and then filled with argon through a needle bulb. Typical working pressures for the ICPs used in this study were 40 and 169 Pa.

C. Double-probe measurement system

In order to check the accuracy of the THz-TDS based electron-density measurement method, we have also measured the electron densities of the ICPs with a double probe.[8–11] Figure 3 shows the locations of probe measurements. In the probe configuration of Fig. 3(a), a probe is inserted from a port on the bottom flange of the cross in such a way that the THz-TDS can be performed in the presence of a probe inside the chamber. In the configuration of Fig. 3(b), a probe is inserted from a port on Flange 1 of Fig. 2 at the end of the extended horizontal tube. In this configuration, the polyethylene windows shown in Fig. 2 are replaced with stainless steel (SUS) flanges, which mechanically support the probes. In the configuration of Fig. 3(b), therefore, THz waves cannot be transmitted through the chamber as the SUS flanges would block such a transmission. The probe insertion depth is measured from the surface of the connection flange (Flange 2 of Fig. 2) near the RF antenna, not from the SUS flange that supports the probe.

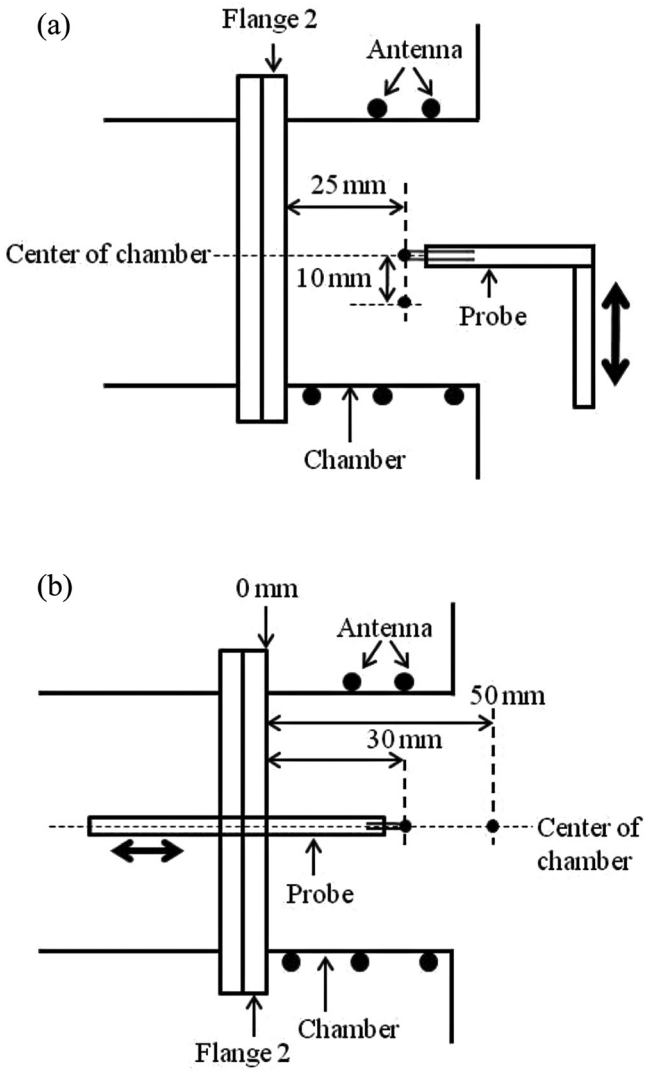

FIG. 3. Schematic diagrams of the probe setups. In (a) the probe is inserted from a port on the bottom flange of the cross in such a way that the THz–TDS can be performed in the presence of the probe inside the chamber. In (b) the probe is inserted from a port on Flange 1 in Fig. 2 of the extended horizontal tube. The horizontal location of the probe measurement is indicated by the distance measured from the surface of the connection flange (Flange 2) near the RF antenna that generates plasmas.

IV. EXPERIMENTAL RESULTS

A. THz-TDS experimental procedures

As we discussed earlier, information on the average electron density can be obtained from the phase shift of the THz wave pulses that pass through the plasma. The phase shift as a function of the wave frequency can be obtained from the Fourier components of two sets of THz EM pulses, one of which passes through the chamber without a plasma and the other with a plasma. The Fourier components (i.e., frequency spectra) of the THz EM waves are derived directly from the time-dependent signals obtained at the detector. In experiments, first the plasma chamber is filled with argon gas and the frequency spectra of THz pulses that pass through the chamber are obtained as reference spectra. Second, an argon plasma is generated at the same gas pressure and the frequency spectra of THz pulses that pass through the plasma are then obtained, which we call phase-shifted spectra. Both reference and phase-shifted spectra are obtained for each discharge with a different set of plasma control parameters (i.e., pressure and RF power in this study). In this study, the RF power was varied from 22 to 142 W.

It should be noted that the optical path in the plasma chamber can change due to the expansion of the plasma chamber by heat when the input power is sufficiently high. In this study, the reference THz signals were taken right after the plasma was turned off and therefore, the effect of chamber expansion is taken into consideration for the phase shift measurements.

In our experiments, the time-dependent wave form of THz pulses was recorded with 2500 data points for 330 ps, i.e., at 0.133 ps intervals, which was then transformed into the frequency-domain amplitude spectra (i.e., frequency spectra) by fast Fourier transformation (FFT). The maximum frequency reliably obtained for the spectra was 3.75 THz with a spectral resolution of 0.003 THz.

B. THz-TDS measurement results

Under the experimental conditions reported in this article, when we generate a plasma by increasing the RF input power from zero to the designated power (22 to 142 W) with optimal impedance matching, we always observe a clear transition from a relatively dark (E-mode) plasma to a highly bright (H-mode) plasma. This observation suggests that we successfully generate high-density ICPs in our system.

A sample of a phase-shifted wave form obtained from THz pulses passing through an argon ICP (40 Pa, 35 W), together with the reference wave form (i.e., a wave form of THz pulses passing through a 40 Pa argon gas *without plasma*), is shown in Fig. 4. The difference in the two wave forms reflects the dielectric nature of the plasma.

The small peaks at about 310 ps seen in Fig. 4 are reflection signals by the hyper-hemispherical silicon lens on the emitter. We use data on the wave forms only up to 312 ps (and digitized to 2348 points) to avoid the reflection signals. Reflection signals by the polyethylene windows appear even after those by the hyper-hemispherical silicon lens.

The phase shift of a THz pulse due to the presence of a plasma can be obtained by the FFT in the time of the electric field wave forms. Figure 5 shows the phase shifts as functions of the wave frequency obtained from our system for plasmas generated with different RF powers at 40 Pa. In Fig. 5, it is clearly seen that the gradient of each curve is –1, i.e., the phase shift is inversely proportional to the frequency, which is consistent with Eq. (4). The fitting curve is indicated by a broken line at each input power.

Shown in Fig. 6 are the electron densities obtained from the fitting of the theory curve of Eq. (4) to the phase shift obtained from THz-TDS for Ar discharges at 40 (Fig. 6(a)) and 169 Pa (Fig. 6(b)) as functions of input power. The plasma length, L, that appears in Eq. (4) is assumed to be 70 mm, based on the visual inspection of the plasma in the chamber. The plasma density profile measurement that we shall show later also suggests that this assumption is reasonable. For the sake of simplicity, $L = 70$ mm is assumed under all conditions presented in this paper. In order to examine the effect of the disturbance caused by the presence of a double probe, the THz-TDS was also performed when a probe is left inserted at the center of the plasmas in the configuration of Fig. 3(a). The open circles and squares in Fig. 6 indicate the electron densities measured by THz-TDS in the presence of a probe. On the contrary, the filled circles and squares indicate the electron densities measured by THz-TDS in the absence of a probe. It is seen that the disturbance caused by

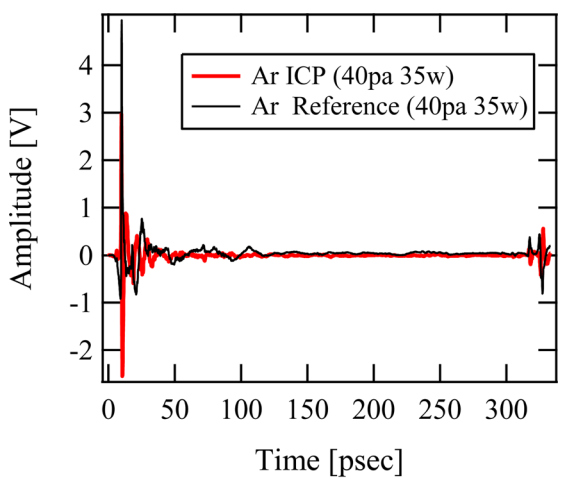

FIG. 4. (Color online) Temporal variation of the THz pulses that pass through an argon ICP at 40 Pa driven by an RF input power of 35 W [i.e., the sample signal, denoted by the gray line (red line online)] and an argon gas only (i.e., the reference signal, denoted by the broken line) at the same pressure.

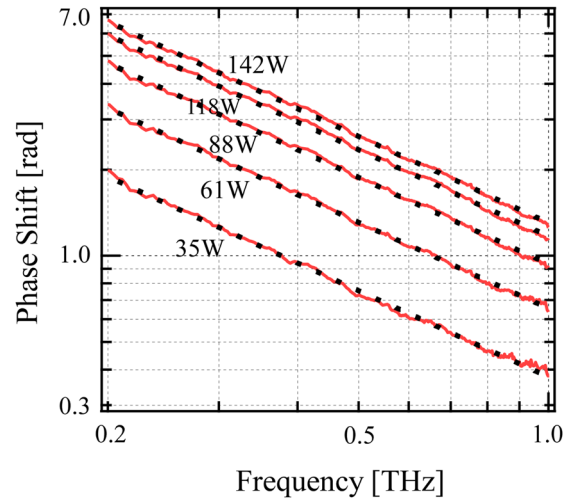

FIG. 5. (Color online) Phase shift of THz pulses that pass through argon ICPs at 40 Pa driven by various input RF power. The solid curves represent the measured phase shifts and the broken lines are fitting curves based on Eq. (4).

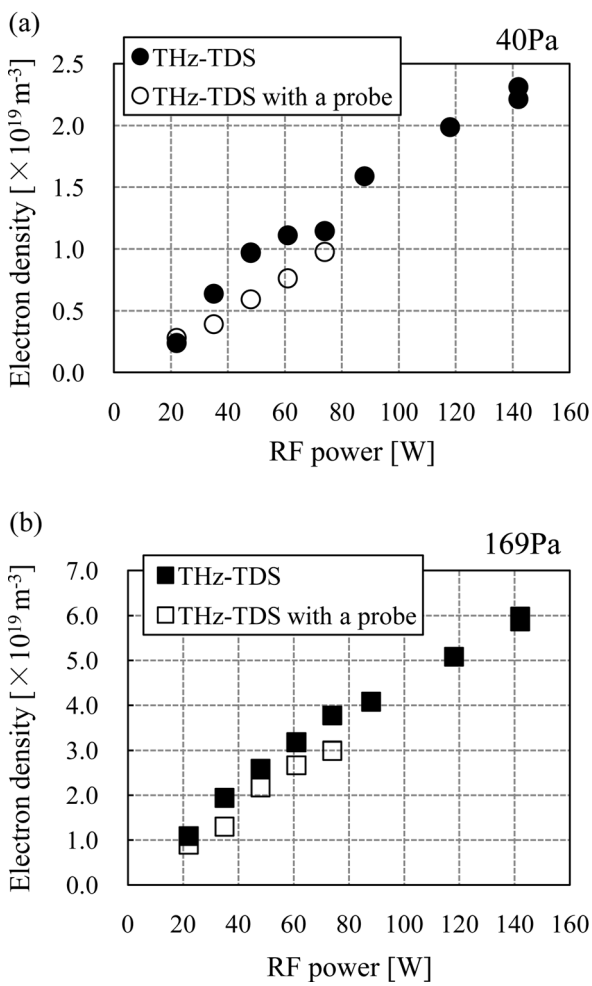

FIG. 6. Electron densities of argon ICPs obtained from the THz-TDS as functions of the input RF power at (a) 40 Pa, and (b) 169 Pa. Here, the filled circles and squares represent data taken in the absence of a probe in the chamber, whereas empty circles and squares in the presence of a probe at the center are the same as in the configuration of Fig. 3(a).

a probe has only minor effects on the line averaged electron densities.

Based upon the electron density data of Fig. 6, we now check the validity of the assumptions made to derive Eq. (4). Figure 6 shows that, under the conditions we employed here, the electron density varies approximately from 2×10^{18} m^{-3} to 6×10^{19} m^{-3}, which translates into the electron plasma frequencies, ω_p, from 0.08 to 0.44 THz. Since the frequency range of the THz-TDS system we used for this study was up to about 3 THz, the assumption, $\omega^2 \gg \omega_p^2$ was well satisfied for our analysis. The electron-Ar neutral collision frequencies expected at 40 and 169 Pa (at room temperature with, for example, 5 eV electrons) are approximately 1.6 and 6.8 GHz. Therefore, the assumption, $\omega^2 \gg \nu^2$, used to derive Eq. (2) from Eq. (1) is also clearly justified.

C. Comparison with probe measurements

In order to confirm that the line averaged electron densities obtained from THz-TDS are in line with the estimates by other means, we have compared the electron densities obtained from THz-TDS with those obtained from double probe measurements under the same plasma conditions. Under the conditions for Ar discharge at 169 Pa shown in Fig. 6, the heat load to the probe was so high that we could not insert the probe (the external tube of which was made of quartz) into the plasma without damaging the probe. Therefore, the comparison was made only for the cases at a gas pressure of 40 Pa. This already suggests the usefulness of THz-TDS as an electron-density diagnostic technique, which can be applied to a plasma whose electron density cannot be measured by the traditional probe-based method.

At a pressure of 40 Pa, the electron-neutral mean free path is about 1 mm, whereas the electron Debye length for a plasma of 10^{12} cm^{-3} in electron density and 2 eV in electron temperature is about 10^{-5} m. Since the Debye length is much shorter than the mean free path, the sheath formed around the probe tip (whose diameter and length are 0.3 mm and 1 mm, respectively) may be considered nearly collisionless. In the double probe measurement presented here, we use a standard method of evaluating the electron density and temperature for collisionless plasmas. However, we do not intend to prove here that the application of the collisionless-plasma probe theory can be justified for our Ar ICP generated at 40 Pa. Instead we demonstrate here that such a formal application of a collisionless-plasma probe theory to the measured probe data is possible even at 40 Pa and compare the results with the THz-TDS data. More discussion on the probe measurement at 40 Pa is given in the Appendix.

Figure 7 shows a comparison of electron densities obtained from THz-TDS (circles) and a double probe (triangles) for discharges at 40 Pa at various input powers. The THz-TDS was performed in the presence of the probe at the center, as in Fig. 3(a). The THz-TDS data are the same as those denoted by open circles in Fig. 6(a). Although the cause of the discrepancy between the data sets of the THz-TDS and probe measurements is not completely identified, given the uncertainties associated with probe measurement at this relatively high collisionality (at 40 Pa) and the assumed length, L, for THz-TDS, the agreement between the electron densities obtained from the two different measurements shown here should be considered satisfactory.

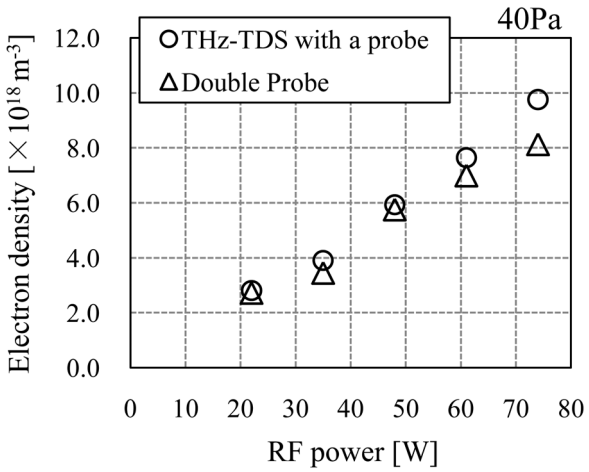

FIG. 7. Comparison of electron densities obtained from THz-TDS (circles) and a double probe (triangles) for discharges at 40 Pa at various input power. The THz-TDS was performed in the presence of the probe at the center, as in Fig. 3(a). The THz-TDS data are the same as those denoted by open circles in Fig. 6(a).

We have also used probe measurements to estimate electron density profiles. With the use of the probe configurations of Fig. 3(a), the electron densities at the center (triangles) and 10 mm away from the center (squares) in the radial direction were obtained from double probe measurement as functions of the input power, which are summarized in Fig. 8. The gas pressure was 40 Pa and the probe was set at 25 mm away from the connection flange (Flange 2 of Fig. 2) in the axial direction. Incidentally, data given by triangles here are not exactly the same as the probe data shown in Fig. 7, due to statistical variations of data taken on different occasions under the same external conditions. The results indicate that the plasma is relatively peaked at the center.

Figure 9 shows the electron densities as functions of input power obtained from a double probe at two different

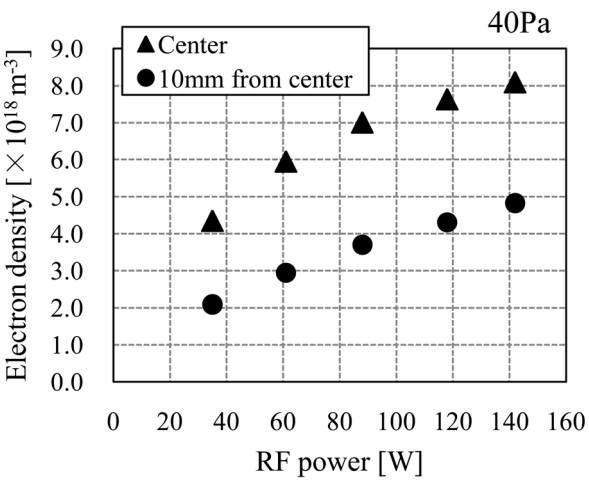

FIG. 8. Electron densities at the center (triangles) and 10 mm away from the center (squares) in the radial direction obtained from double probe measurements as functions of the input power. The gas pressure is 40 Pa. The probe configurations are given in Fig. 3(a).

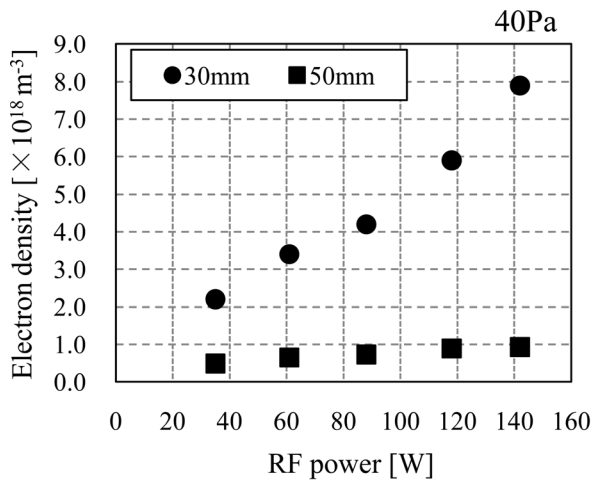

FIG. 9. Electron densities obtained from double probe measurements for discharges at 40 Pa as functions of the input power. The probe was located at 30 mm (circles) and 50 mm (squares) away from the connection flange (Flange 2), as in Fig. 3(b).

axial locations, i.e., at 30 mm (circles) and 50 mm (squares) away from the connection flange (Flange 2). The pressure was 40 Pa and the probe was radially located at the center, as in Fig. 3(b). It should be noted that the presence of the probe may have disturbed the plasma especially when it is inserted from Flange 1 up to the location of 50 mm measured from Flange 2.

To minimize the disturbance of the plasma by probe insertion, we have also performed an electron density measurement with a probe inserted from a port on Flange 3 of Fig. 2, which is given in Fig. 10. In this figure, a probe is radially placed at the center and its axial (horizontal) position is indicated by the distance from the surface of Flange 2 near the RF antenna, as shown in Fig. 3(b). For this measurement,

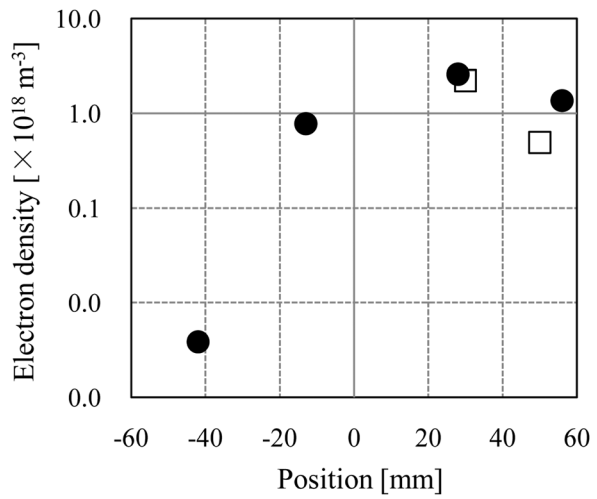

FIG. 10. The electron density profile (filled circles) in the axial (horizontal) direction for an Ar ICP at 40 Pa with 35 W RF input power obtained from double-probe measurements. The axial positions are indicated by a distance measured from the Flange 2 surface near the RF antenna, as indicated in Fig. 3(b). The electron density data at 35 W given in Fig. 9 are shown by empty squares, as a comparison. The densities indicated by filled circles at positive axial locations were measured by a probe inserted from a port on Flange 3 of Fig. 2, unlike data given in Fig. 9 (indicated here by empty squares), for which the probe was inserted from a port on Flange 1.

the gas pressure was 40 Pa and the input power was 35 W. The electron densities (denoted by filled circles) at negative axial positions were measured by a probe inserted from a port on Flange 1, whereas the electron densities (denoted by filled circles) at positive axial positions were measured by a probe inserted from a port on Flange 3. For comparison, the electron density data at 35 W given in Fig. 9 are indicated by empty squares. The profile data given in Fig. 10 is consistent with our assumption on the plasma length, $L = 70$ mm.

V. SUMMARY AND CONCLUSIONS

In this study, line-averaged electron densities of low-pressure Ar ICPs were measured by THz-TDS. The plasmas were driven by RF power with a frequency of 13.56 MHz at gas pressures of 40 and 169 Pa. The input RF power was varied from 22 to 142 W. Some of the measured electron densities were compared with those obtained from double-probe measurement and found to be in reasonable agreement, given some uncertainties associated with both measurement methods.

The THz-TDS technique for electron-density measurement that we have employed in this work is essentially the same as what Jamison *et al.*,[2] Kohler *et al.*,[3,4] or Mics *et al.*[5] employed in their studies on pulsed high-pressure discharges. In their studies, however, their THz-TDS measurements were not compared with those obtained from other means since there is practically no other established method to measure electron densities for high-pressure transient plasmas. Since we applied this method to ICPs whose densities can be also estimated by probe measurement with relative ease, we were able to corroborate the validity of THz-TDS as an electron density measurement method by comparing the two methods. In this way, THz-TDS has been shown to provide reliable estimates of line-averaged electron densities.

Even for ICPs at relatively low pressures, the plasma density and heat load can increase as the input power increases. Indeed in our experiments at 169 Pa, probe measurement could produce no electron density data because the high heat load of the system damaged the probe. On the contrary, since the THz-TDS measurement is not interfered with by high gas temperature, it can serve as an alternative technique for electron-density measurement to probe measurement under such conditions.

For high pressure plasmas, THz-TDS is even more suitable as a method for electron-density evaluation. For example, pulsed discharges at near atmospheric pressure are typically small and do not allow a probe to be inserted without being affected by the presence of a probe. Microwave interferometry (which is widely used for electron-density measurement of low-pressure fully ionized plasmas) cannot be used, either, since typical wavelengths of microwaves are in the range of a few cm, which are typically much larger than the sizes of atmospheric-pressure plasma discharges. As long as a plasma has a sufficient size, at least in a particular direction, so that the phase shift given in Eq. (4) is observable for THz waves, THz-TDS is applicable for the electron density evaluation of plasmas at high pressures. As Eq. (4) indicates,

if the electron density is sufficiently high, the restriction coming from the plasma size, L, becomes even less severe.

Although the time resolved measurement of electron densities is also possible by THz-TDS (as demonstrated by Jamison *et al.*,[2] Kohler *et al.*,[3,4] and Mics *et al.*[5]), we only measured the time (and line) averaged electron densities of ICPs in this study since the bulk density profile of an ICP is considered to be nearly constant in time during the discharge. However, for example, the electron density in the sheath region of a capacitively coupled plasma driven by an RF frequency is known to oscillate in time with the RF frequency, so if the THz beam diameter can be made sufficiently smaller than the sheath width, one may be able to evaluate the time evolution of the sheath density. Time resolved measurement of electron densities in RF-driven plasmas will be the subject of a future study.

APPENDIX: DOUBLE PROBE MEASUREMENTS OF ARGON ICPS

In this study, we have evaluated the electron density of an Ar ICP at 40 Pa, using a double probe. At 40 Pa, the electron-neutral mean free path is approximately 1 mm, whereas the electron Debye length for a plasma of 10^{12} cm^{-3} in electron density and 2 eV in electron temperature is about 10^{-5} m. Since the Debye length is much shorter than the mean free path, the sheath formed around the probe tip may be considered nearly collisionless.

Although we do not intend to prove that collisionless probe theory is valid for our Ar ICP plasmas at 40 Pa, we demonstrate here that the current-voltage curves that we obtain for such plasmas are similar to what one would expect for collisionless plasmas.

Figure 11 shows the relation between the probe current, I_p, and the applied voltage to the probe, V_d, obtained from a probe measurement of argon ICP with a gas pressure of 40 Pa and an RF input power of 35 W. The probe tip was located at the center of the plasma, as indicated in Fig. 3(a). The surface area of the probe tip is approximately 1×10^{-6} m^2 and the applied voltage to the probe was varied from −16 V to +16 V. For a collisionless plasma, the electron temperature, T_e, can be estimated[9] from the relation,

$$T_e = \frac{e}{k} \frac{\sum I_i}{4\left(\frac{dI_P}{dV_d}\right)_{V=0} - 3.28\left(\frac{dI_P}{dV_d}\right)_{sat}},$$

where e is the electron elementary charge, k is the Boltzmann constant, $(dI_p/dV_d)_{V=0}$ is the gradient of I_p at $V_d = 0$, $(dI_p/dV_d)_{sat}$ is the gradient of I_p in the saturation region of I_p, and ΣI_i is the sum of the absolute values of the probe currents obtained from the cross points for the current axis (i.e., y axis) and the tangential lines of saturated probe currents, as indicated in Fig. 11. With the obtained electron temperature, T_e, the electron density, n_e, can be calculated from the relation,

$$N_e = \frac{I_0}{0.61 \cdot eS}\left(\frac{m_i}{kT_e}\right)^{1/2},$$

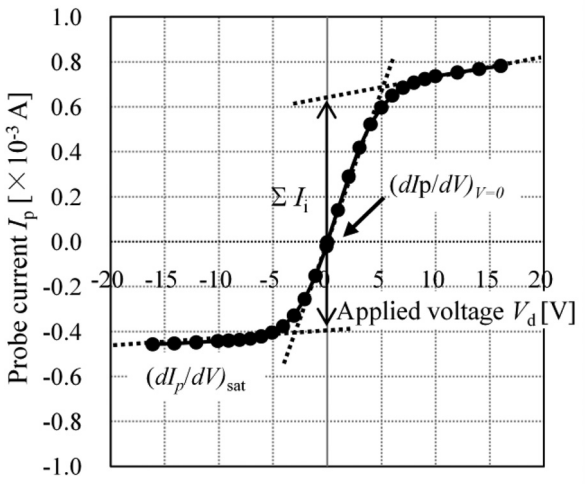

FIG. 11. The relation between the probe current, I_p, and the applied voltage to the probe, V_d, obtained from a probe measurement of argon ICP with a gas pressure of 40 Pa and an RF input power of 35 W. The probe tip was located at the center of the plasma, as indicated in Fig. 3(a).

where I_0 is the ion current at $V_d = 0$, S is the surface area of the probe ($S = 1 \times 10^{-6}$ m^2 in our case) and m_i is the ion mass.[12]

The curve shown in Fig. 11 is smooth and follows a shape that the probe theory for collisionless plasma predicts. Assuming that the plasma is collisionless and applying the relations above, we obtain from Fig. 11 the electron temperature and density as 2.0 eV and 3.5×10^{18} m^{-3}.

ACKNOWLEDGMENTS

This work was supported in part by Grants-in-Aid for Scientific Research from the Ministry of Education, Culture, Sports, Science and Technology (MEXT) of Japan. The visit by V.R. to Osaka University was supported by the student exchange program between Osaka University and the University of Strasbourg.

[1]D. H. Auston, K. P. Cheung, and P. R. Smith, Appl. Phys. Let. **45**, 284 (1984).
[2]S. P. Jamison, J. Shen, D. R. Jone, R. C. Issac, B. Ersfeld, D. Clark, and D. A. Jaroszynski, J. Appl. Phys. **93**, 7 (2003).
[3]B. H. Kolner, P. M. Conklin, R.A. Buckles, N.K. Fontaine, and R. P. Scott, Appl. Phys. Lett. **87**, 151501 (2005).
[4]B. H. Kolner, R. A. Buckles, P. M. Conklin, and R. P. Scott, IEEE J. sel. Top. Quantum Electron. **14**, 505 (2008).
[5]Z. Mics, F. Kadlec, and P. Kuzel, J. Chem. Phys. **123**, 104310 (2005).
[6]M. Hangyo, T Nagashima, and S Nashima, Meas. Sci. Technol. **13**, 1727 (2002).
[7]M. Tani, S. Matsuura, K. Sakai, and S. Nakashima, Appl. Opt. **36**, 7853 (1997).
[8]E. O. Johnson and L. Malter, Phys. Rev. **80**, 58 (1950).
[9]T. Dote, Jpn. J. Appl. Phys. **7**, 964 (1968).
[10]J. Aorim, H. S. Maciel, and J. P. Sudano, J. Vac. Sci. Technol. B **9**, 362 (1991).
[11]V. A. Godyak, R. B. Piejak, and B. M. Alexandrovich, Plasma Sources Sci. Technol. **11**, 525 (2002).
[12]S.-L. Chen and T. Sekiguchi, J. Appl. Phys. **36**, 2363 (1965).